Numerical Simulation of the Stent Expansion Process based on the Hemodynamic Characteristics of Bidirectional Fluid-structure Coupling

Siyu Bai (493444596@qq.com)
College of Aerospace and Civil Engineering, Harbin Engineering University, Harbin, China
Hong Li
College of Aerospace and Civil Engineering, Harbin Engineering University, Harbin, China
Li Li
College of Materials Science and Chemical Engineering, Harbin Engineering University, Harbin, China

Research Article

Keywords: coronary stent, finite element methods, finite volume methods, expansion, bidirectional fluid-structure coupling

Posted Date: December 28th, 2020

DOI: https://doi.org/10.21203/rs.3.rs-129732/v1

Numerical simulation of the stent expansion process based on the hemodynamic characteristics of bidirectional fluid-structure coupling

Siyu Bai[1*], Hong Li[1*] , Li Li[2]

[1]College of Aerospace and Civil Engineering, Harbin Engineering University, Harbin, China

[2]College of Materials Science and Chemical Engineering, Harbin Engineering University, Harbin, China

*** Correspondence:**
Siyu Bai
493444596@qq.com

Keywords: coronary stent, finite element methods, finite volume methods, expansion, bidirectional fluid-structure coupling.

Abstract

Hitherto, research on the fluid-structure coupling of coronary stents has mostly considered the state after stent expansion following implantation. However, the factors and how they affect stent expansion are as yet, unclear. To further investigate stent expansion, this paper proposes a model combining balloon, stent, and blood using Solidworks. Thereafter, a co-simulation using ANSYS Workbench is implemented using the methods of finite element and finite volume, to analyze bidirectional fluid-structure coupling during the expansion of a balloon-expandable stent, for periodically varying blood loads. By comparing the blood flow rate in the vessel, pressure on the endovascular wall, and the pressure and stress on the stent system at different points in time, it can be seen that the higher the blood flow rate, the greater the pressure on the endovascular wall and stent system. Furthermore, the larger the volume of the implant, the greater the maximum blood flow rate and maximum pressure on the endovascular wall, and the more drastic the change along the axis. In summary, the results of the present study indicate that the stent expansion process has a significant effect on the blood flow rate and pressure on the vascular wall; however, the impact of blood load on stent stress can be ignored.

1 Introduction

Coronary heart disease is characterized by the narrowing or blockage of coronary artery lumina due to atherosclerotic lesions and is currently one of the most common diseases affecting human health (Lim et al.,2007; Koens et al.,2015). In recent years, coronary stent interventions have been considered to be important in the treatment of coronary heart disease, since they are deemed as being very safe and are associated with less trauma than other interventions(Zhang and Liu,2007; Wei et al.,2010; Wu et al.,2014). The expansions of coronary stents following their deployment often adversely affect the hemodynamics of patients. In recent years, the interactions between stent expansion and hemodynamics, and the resulting impact on the human body have become the focus of several studies (Qiao and Zeng, 2013; He and Lin, 2015;Bukač et al.,2016; Jiang et al.,2016;Wang et al.,2017; Jang et al.,2018). Computer-based simulation techniques to guide clinical treatment increase the accuracy and efficiency of clinical treatments, and have become one of the most effective

approaches in solving real problems in clinical medicine (Zhang et al.,2000). Among them, numerical simulation is the main method used to study biofluid mechanics models.

The state-of-the-art of studying the hemodynamics of coronary stent interventions involves three techniques: in vitro experiments, in vivo experiments, and numerical simulations. Natarajan et al.(2000) analyzed the effect of stents on blood flow in vessels for periodically changing blood flow rates, using experimental and finite element analysis methods. Ladisa et al. (2003) set up a coupling model of blood, coronary vessels, and stents, analyzed vascular wall shear stress and flow characteristics for stable blood flows, and the maximum diameter of coronary vessels. Seo et al.(2005) combined theoretical hemodynamics with finite element methods, to analyze the dynamics of blood flow through stents in both straight and curved blood vessels. However, due to computational limitations, most studies conducted at the time were based on theoretical derivations and in vivo experiments, and virtual reality simulations were greatly restricted.

With rapid advances in computational technology and the continuous development of finite element methods, numerical simulation has become the primary method for studying coronary stents along with other investigations in biofluid mechanics. Bukač et al.(2016,2019) constructed a stent coupling model after expansion and used simulation techniques to show that the presence of a stent changes the flow pattern in a blood vessel, resulting in a separation and reattachment of blood flow due to obstruction by the stent, and the region of low shear stress thus generated promotes blood retention, which in turn, results in intravascular stent restenosis. Based on this research, they investigated fluid-structure coupling behavior for four different types of stent expansion processes in a curved blood vessel model, to validate the curvature changes of applied stents. Moreover, Jayendirana et al.(2018,2019) applied a Ni-alloy stent with memory for repairing the aorta and analyzed the hemodynamic load on the stent during the repair process using fluid-structure coupling. Furthermore, Leea et al.(2020) established a composite model of blood, blood vessel, and stent, after the stent expansion process. Their model considered blood as an external load on the stent surface, simulated unidirectional coupling of the system during service, obtained pressure on the stent surface, and assessed its mechanical properties. Hitherto most research on stent system hemodynamic characteristics have only considered stents in service in a fully expanded state with no further changes in geometry and position and with limited impact on blood flow. However, the stent expansion process, during which the geometry of a stent changes in real-time and has a significant impact on the periodically changing blood flow, requires further investigation.

The main contribution of this study is the proposition of a model combining a balloon, stent, and blood, using Solidworks software. Thereafter, a co-simulation approach is presented using finite element and finite volume methods to investigate the fluid-structure coupling of a balloon-expandable coronary stent subjected to a periodically changing blood load during the stent expansion process. The blood flow rate and the pressure of the blood on both the stent and vascular wall during the period of research were obtained. Furthermore, the distribution of blood in the stenotic artery in the presence of an expanding stent was compared to that without an implant over the same temporal cycle. The pressure on the stent system due to the impact of a blood load and the stress distribution of the stent during the stent expansion process were also analyzed. From these studies on the changes in blood flow due to stent expansion, a reference and guide for the clinical and surgical treatment of coronary heart disease can be developed.

2 Materials and Methods

2.1 Geometric model

To address the research challenges described above, a balloon-expandable stent system model consisting of a balloon, stent, and blood vessel, was built using the Solidworks 2020 3D modeling platform (see Figure 1). The elements of the model were assembled and then imported into the finite element simulation platform Ansys 2020 R2 for further analysis(Shi et al.,2015). The model for the stent consisted of four groups of sinusoidal-shaped support rings and three sets of straight bridge strips (see Figure 2), that have the advantages of providing better radial support and retraction rates(Timmins et al.,2017). The inner and outer diameters of the stent were 3.3 mm and 3.6 mm, respectively. The thickness of the stent was 0.15 mm with an axial length of 7.72 mm. Each support ring had a length of 2.05 mm, while the length of the bridge strip was 1.67 mm. The balloon was modeled as a thin-walled cylindrical shell with a thickness of 0.01 mm and an outer diameter of 3.3 mm, to fit within the inner diameter of the stent. The blood vessel was modeled as an axially asymmetric segmented cylinder with a total length of 28 mm with a maximum diameter of 6 mm and a minimum diameter of 5 mm. To account for blockages in the blood vessel, a model with a local narrowing was built to simulate the effect of plaque on blood flow. Within the blood flow model, Boolean operations were implemented to remove the corresponding parts of the balloon and stent, with the remaining portion being the fluid model investigated in this study.

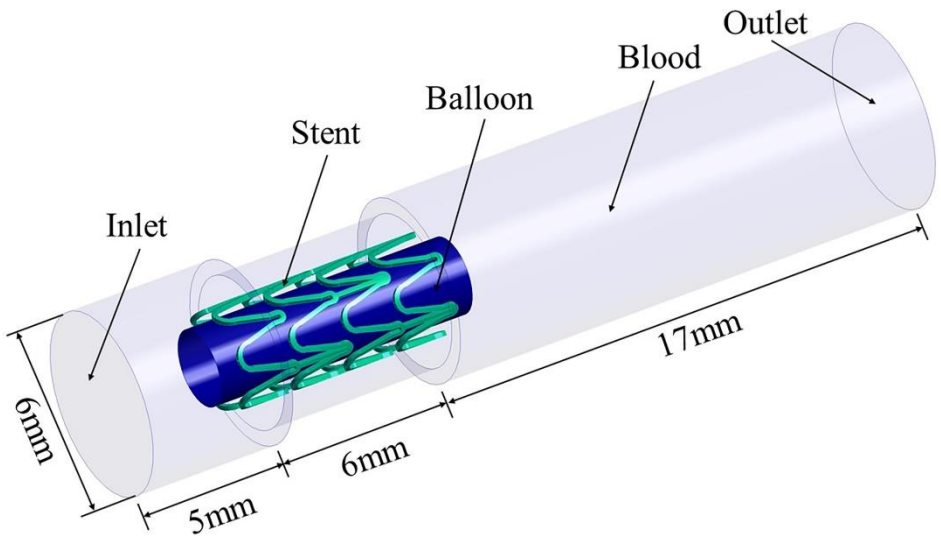

97

98 **Figure 1 A combined model of the balloon, stent, and blood vessel.**

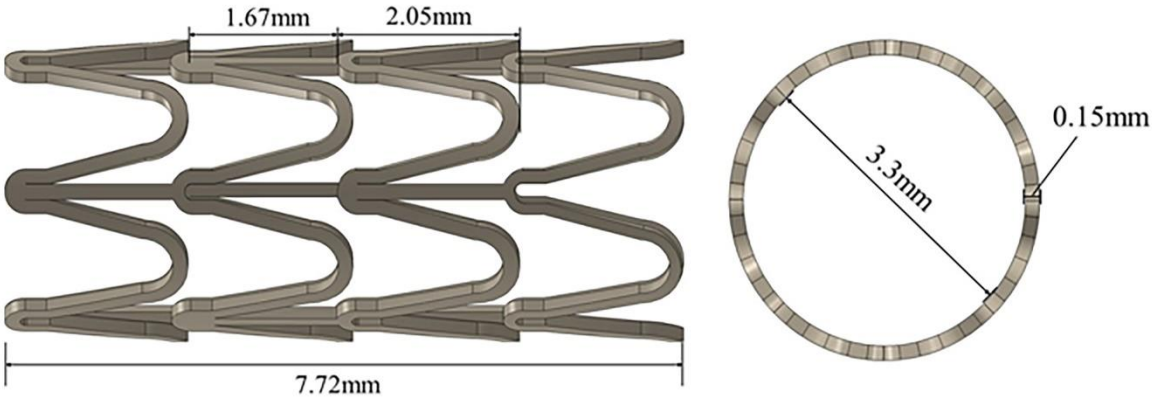

99

100 **Figure 2 Model of the stent.**

101 **2.2 Material characteristics**

102 The material for the stent used in this study was degradable magnesium alloy(Zheng et al.,2017),
103 which was simulated as a bilinear elastoplastic material (Li et al.,2018). The Mooney-Rivlin 2
104 parameters for the balloon were those of a superelastic material (Li et al.,2012) with properties as
105 listed in Table 1. Blood was assumed to be an incompressible Newtonian fluid with a density ρ =
106 1,050 kg /m^3 and a coefficient of viscosity of μ = 0.0035kg•m•s.

Table 1 Material characteristics of the stent and balloon.

Structure	Material	Material model	Elastic Modulus MPa	Poisson's ratio	Density mg/mm³	Yield limit GPa
stent	magnesium alloy	bilinear isotropic	45000	0.35	1.8	0.193
balloon	membrane	hyper elastic	C10 = 1.060 C01 = 0.114	0.49	1.07	

2.3 Meshing and data transfer

The mesh used for the model was divided into two parts, i.e., a solid mesh and a fluid mesh. The stent and balloon were modeled using the solid mesh with the unit type being SOLID186. The unit size for the balloon portion was 0.1 mm, and the unit size for the stent portion was 0.05 mm (see Figure 3(A)). Blood was modeled using the fluid mesh with an overall size of 1.0 mm and a local size of 0.05 mm at the stent and balloon portions of the model (see Figure 3(B)). The coupled system was computed using the Workbench 2020 R2 platform, in which the solid mesh of the balloon and stent was calculated in the Transient Structural module, and the fluid mesh of blood was computed in the Fluent module, with the data from both being exchanged using a system coupler named 'System Coupling'. Additionally, the interface for data transfer was the outer surface of the stent and balloon, and the inner surface of the blood vessel.

Figure 3 Meshes for the balloon-expandable stent (A) and blood (B).

2.4 Boundary conditions and load application

To conform the model to the dynamics of the real situation, the following boundary conditions were set: the solid portion had a cylindrical coordinate system with the axis along the centerline of the balloon and stent which limited the axial and tangential displacements of the balloon to the cylindrical coordinate system. Likewise, the axial and tangential displacements of the six vertices of the support rings in the middle of the stent were also limited to the cylindrical coordinate system. The boundary conditions were set for the fluid portion as follows: since the blood flow in the human body has periodic peaks and troughs(Cebral et al.,2011), the period of the blood flow was set as T = 0.8 s with an average blood flow velocity of v_0 = 0.1 m/s. Moreover, the blood flow velocity at the entrance was simulated as a sinusoidal function: $v = 0.1 + 0.07\sin(7.85t)$(m/s) and the relative pressure at the outlet was set as P_0 = 50 Pa with an inhibiting backflow function. Besides, the portion of blood in contact with the solid part of the model was set as a fluid-structure coupling interface, controlled by the active expansion of the stent and balloon. The outer surface of the blood was considered to be static. The entire simulation process lasted 4s, during which the stent underwent a radial expansion of 0.6 mm from its original size to the inner diameter of the vascular wall. During this process, the blood flow incurred 5 cyclic changes.

2.5 Solutions and configurations

This paper discusses the bidirectional fluid-structure coupling problem during the stent expansion process and incorporates the Transient Structural and Fluent modules mentioned earlier. Finite element methods have been used for the Transient Structural module. Due to large deformations and significant changes to the stiffness matrix, the theory of large deformation was used for the computational process. Besides, the Newton-Raphson method was used to iterate the nonlinear equation. Based on the actual situation, the inertial effect was not considered, and the entire loading process used a quasi-static method. In the Fluent module, finite volume methods were used to study incompressible fluids, whose integral control equation is shown in equation (1) below:

$$\frac{\partial \overline{\mathbf{U}}_{\mathbf{IJ}}}{\partial \mathbf{t}} + \frac{\mathbf{1}}{\mathbf{\Omega_{IJ}}} \oint \mathbf{F} \cdot \mathbf{n}\, \mathbf{ds} - \frac{\mathbf{1}}{\mathbf{\Omega_{IJ}}} \oint \mathbf{F_v} \cdot \mathbf{n}\, \mathbf{ds} = \mathbf{0} \tag{1}$$

where $\frac{1}{\Omega_{IJ}} \oint F \cdot n\, ds$ represents inviscid flux, $\frac{1}{\Omega_{IJ}} \oint F_v \cdot n\, ds = 0$ represents viscous flux, and $\frac{\partial \overline{U}_{IJ}}{\partial t}$ represents the residual fluid. Moreover, $\overline{U}_{IJ} = \frac{1}{\Omega_{IJ}} \iint U\, dV$, represents the average values of mass and momentum. A pressure-based coupled solver named 'Coupled' was used to solve both the continuity and momentum equations, and the discretization gradient used for interpolation was obtained using the least-squares method.

3 Results

3.1 Blood flow rate and distribution

The second cycle (0.8~1.6 s) of blood flow is studied in this section. To obtain representative results, streamline diagrams for the blood flow rate at the initial time (0.8 s), peak time (1.0 s), and the trough time (1.4 s) have been analyzed (see Figure 4). Simultaneously, to study the effect of the stent system on the blood flow rate and distribution, a stent-free blood vessel subjected to the same conditions was used as the control group for the simulations (see Figure 5). Blood flow rate data was calculated at 20 time-points distributed evenly over 0.8~1.6s to obtain a line chart showing the trend of the maximum flow rate with and without implants (see Figure 6).

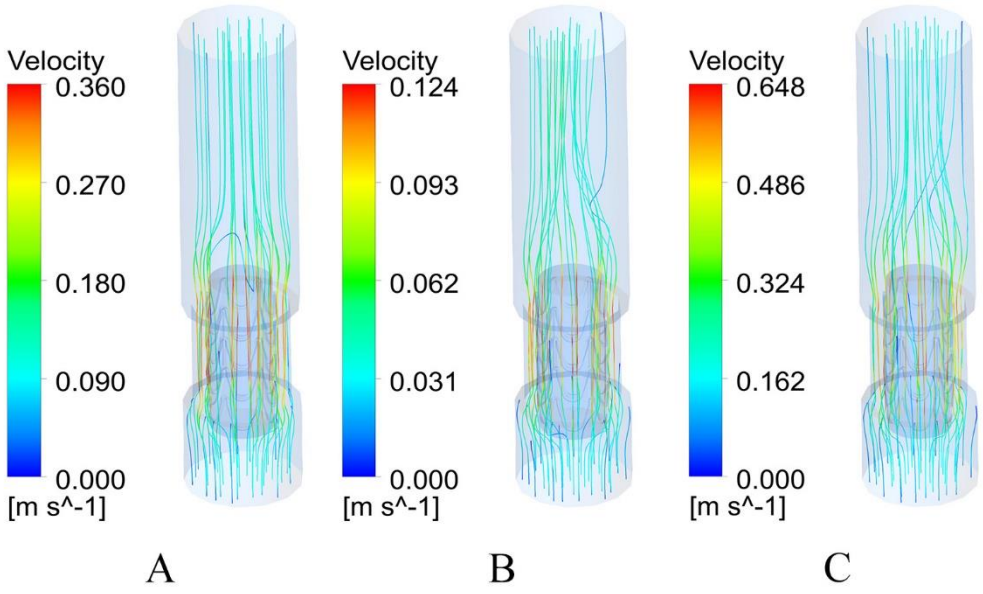

164

165 **Figure 4 Blood flow velocity streamline diagram during stent expansion at t = 0.8 s（A）, 1.0**
166 **s(B), and 1.4 s(C).**

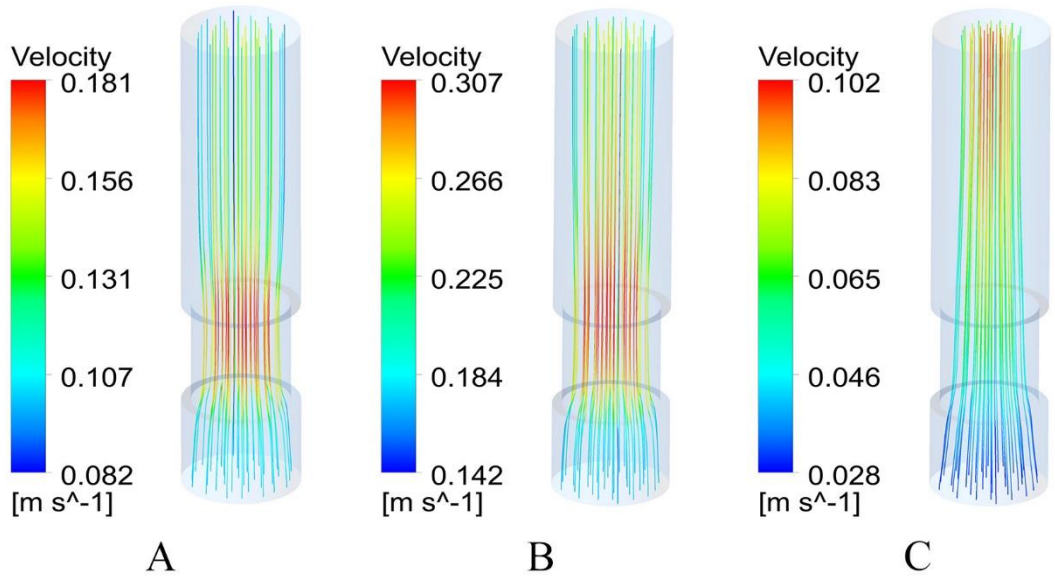

167

168 **Figure 5 Blood flow velocity streamline diagram without stent at t = 0.8 s(A), 1.0 s(B), and**
169 **1.4 s(C).**

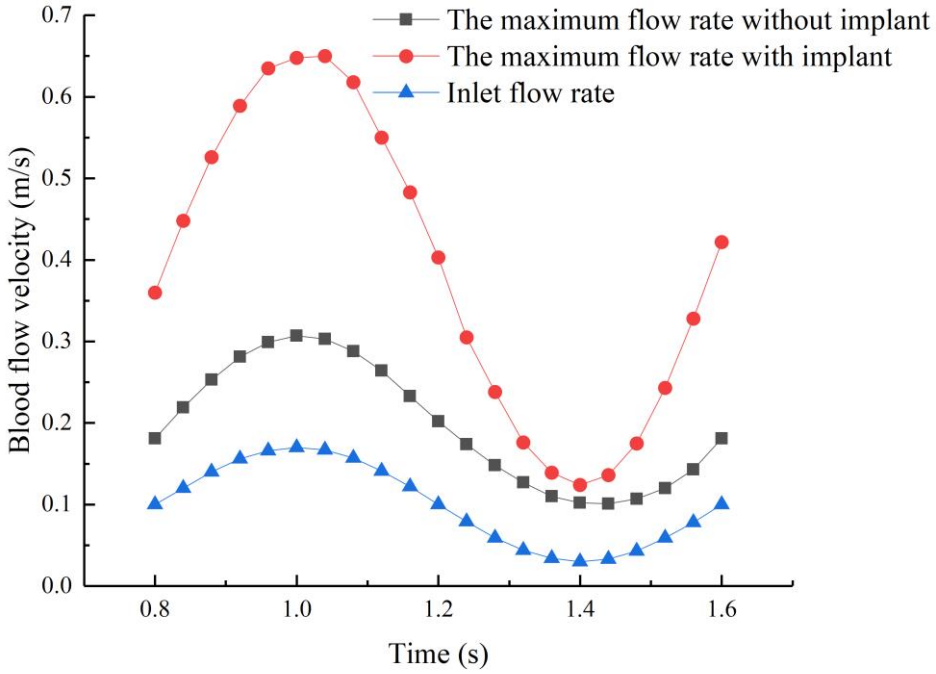

Figure 6 Inlet blood flow rate, and maximum blood flow rate with and without implant at 0.8~1.6s.

It can be seen from Fig. 4 that the maximum blood flow rate at the vascular stenosis at each time point is about 4 times that at the entrance due to the presence of the balloon and stent. Moreover, the blood flow is disturbed over a small region downstream of the implant but returns to a normal streamline flow thereafter. Comparing Figure 4 and Figure 5 shows that for a given time point with the same inlet blood flow rate, the maximum blood flow rate at the stenosis is significantly increased in the presence of the balloon and stent. At the initial and peak time points, the maximum flow rate at the stenosis is twice that without the implant when the blood flow rate is larger. From Figure 6 it is observed that the maximum blood flow rate is consistent at the entrance, with or without an implant.

3.2 Pressure on endovascular wall

Changes in blood flow rates affect the pressure on endovascular walls, which in turn, affect the internal environments of blood vessels and have a direct impact on human health. To further investigate these effects, a cloud diagram of the pressure on a vascular wall at the initial time (0.8 s), peak time (1.0 s), and trough time (1.4 s) of the second cycle has been analyzed in this section (see Figure 7). Also, to study the effects of the stent system on vascular wall pressure, the corresponding pressure on a vascular wall without a stent for the same conditions was used as the control during the computational process (see Figure 8). To explore the trends in vascular wall pressures, the pressures were calculated at 20 time-points distributed evenly during 0.8~1.6 s to obtain a line chart of the maximum pressure with and without implants (see Figure 9).

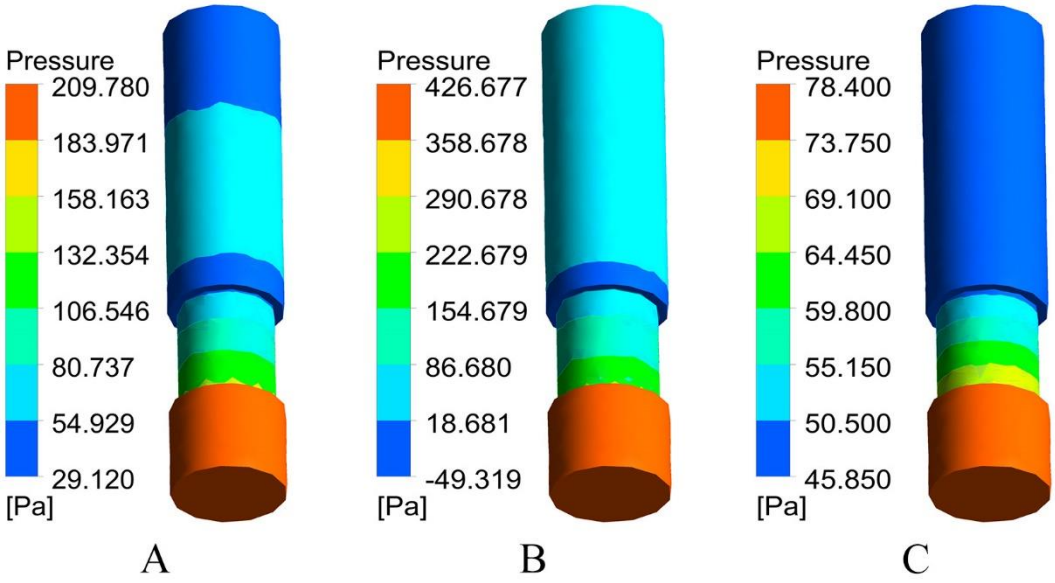

191

192 **Figure 7 Pressure distributions at the endovascular wall during stent expansion at t = 0.8 s(A),**
193 **1.0 s(B), and 1.4 s(C).**

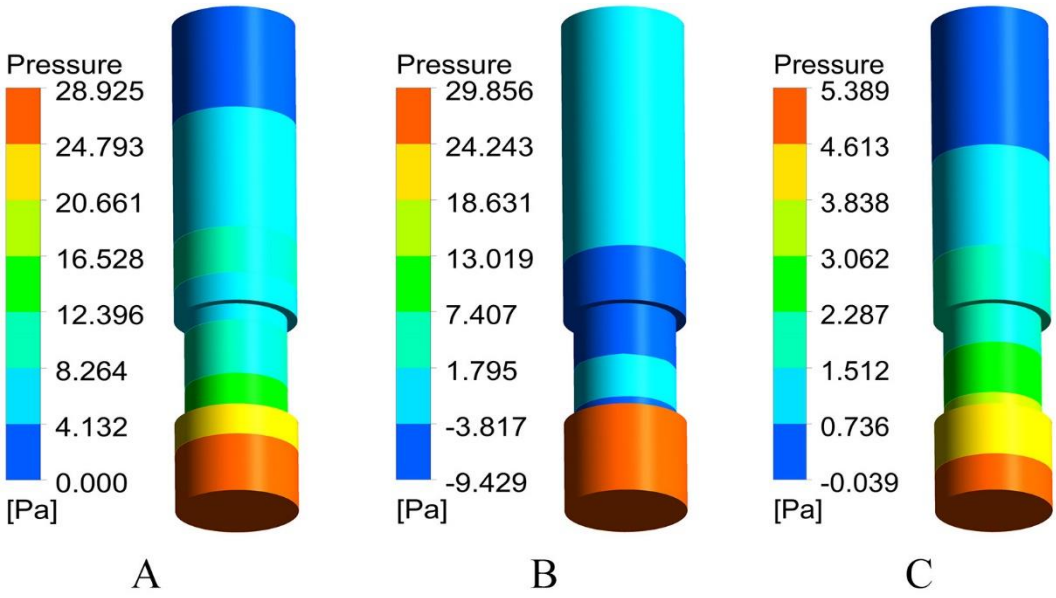

194

195 **Figure 8 Pressure distributions at the endovascular wall at t = 0.8 s(A), 1.0 s(B), and 1.4 s(C)**
196 **without stent.**

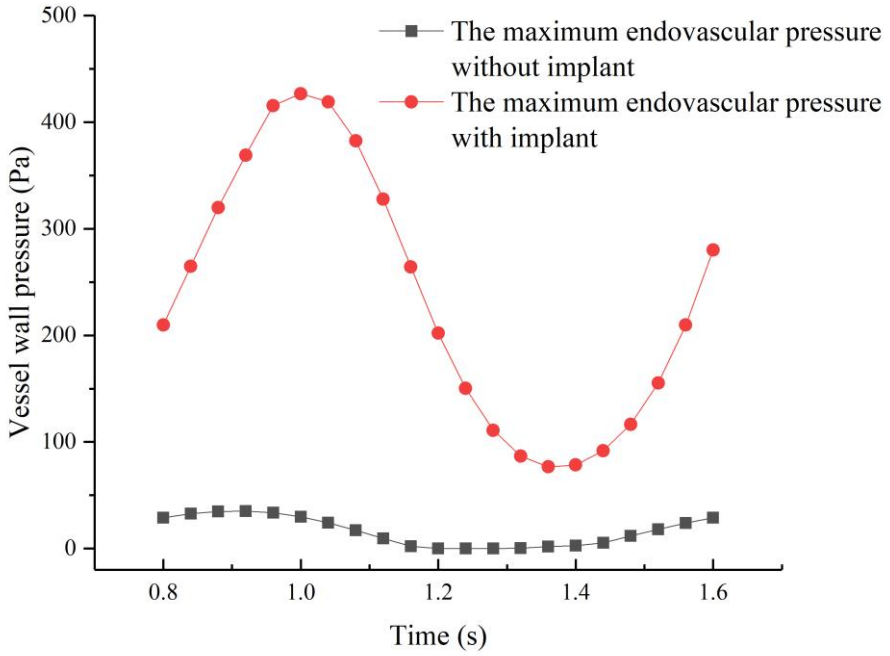

Figure 9 Maximum pressure on the endovascular wall during 0.8~1.6 s with and without implant

It can be seen from Figure 7 that the maximum pressure of blood on the vascular wall increases as the blood flow rate increases, which also leads to an increase in the pressure gradient, and the pressure along the axis of the vascular wall drops rapidly. When the blood flow rate is high, a zone of negative pressure develops at the junction of the stenotic and non-stenotic regions of the blood vessel. A comparison of Figure 7 and Figure 8 shows that, for the same inlet blood flow rate, the presence of an implant can lead to a sharp increase in pressure on the vascular wall due to the modified blood flow. Moreover, this increase in endovascular wall pressure is of several orders of magnitude at the entrance and the stenotic region. Besides, Figure 9 shows that the trend of the maximum pressure on the endovascular wall is consistent with the trend of the blood load due to the implant. In the absence of an implant, the pressure on the endovascular wall is smaller, without any observable changes in the maximum pressure, due to a low blood flow rate.

3.3 Pressure on stent system and stress distribution

When flowing blood initially encounters an implanted stent, the resulting pressure generated on its surface causes the stent to expand. This expansion of the stent can also deform its structure and alter the internal stress. In this section, cloud diagrams of the pressure on the stent system at the initial time (0.8 s), peak time (1.0 s), and trough time (1.4 s) in the second cycle have been analyzed (see Figure 10). Also, the Von-Mises effective stress is obtained for the stent, from which the effect of the blood load on the internal force of the stent is evaluated (see Figure 11). The maximum, minimum, and average stress of the stent during 0.8~1.6 s are shown in Figure 12.

It can be seen from Figure 10 that the pressure of blood on the stent and balloon increases as the blood flow rate increases, and that the pressure gradient increases as well, while the pressure along the axis drops rapidly. This phenomenon is similar to the effect of blood pressure on the endovascular wall. Furthermore, the expansion distance of the stent is proportional to time. It can be seen from Figure 11 that, as time increases, the stent expansion becomes progressively larger, and that its internal stress increases accordingly. For the same time point, the maximum stress appears at the bend with the most change in the geometric angle, while the minimum stress appears at the straight bridge strip. Figure 12 shows that the maximum, minimum, and average stress of the stent are proportional to time, during the stent expansion process.

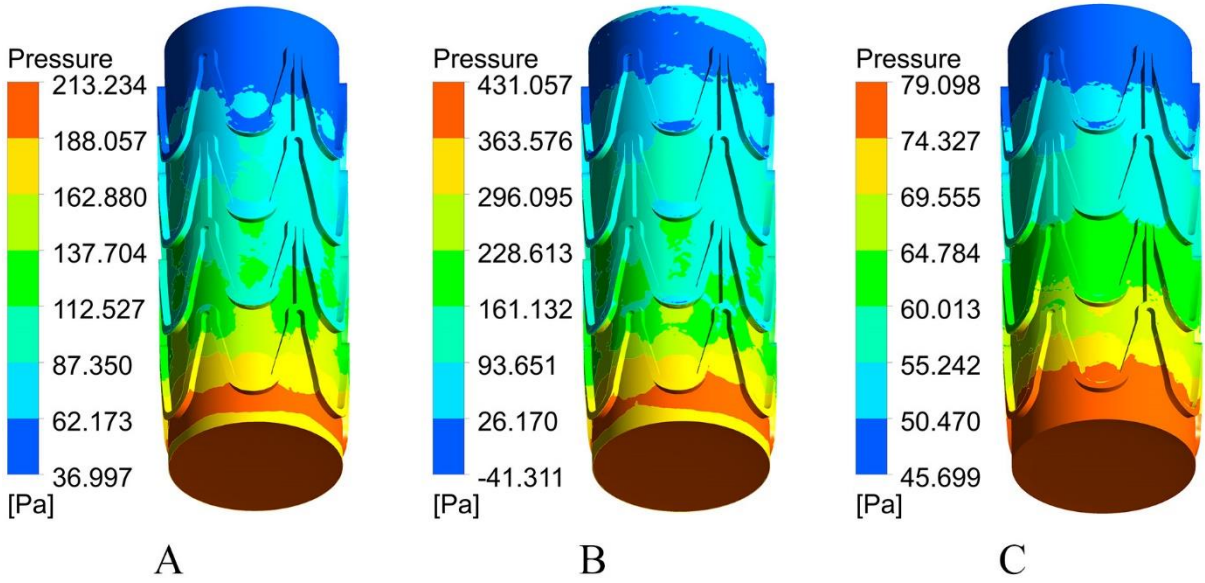

229

230 **Figure 10 Pressure distribution of the stent system at t = 0.8 s(A), 1.0 s(B), and 1.4 s(C).**

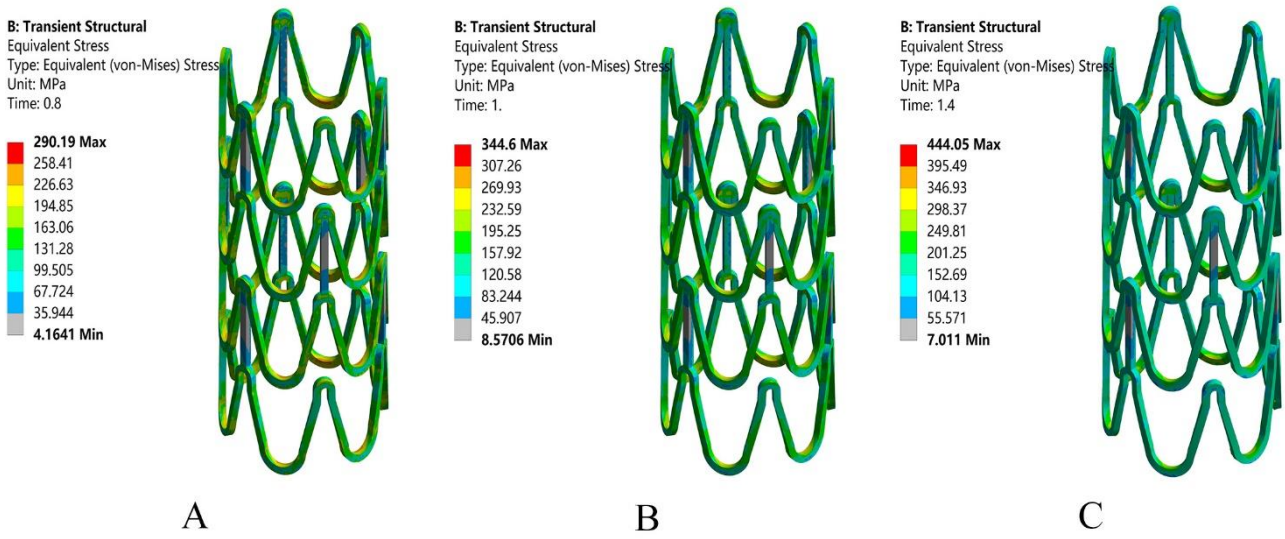

231

232 **Figure 11 Equivalent stresses of the stent at t = 0.8 s, 1.0 s, and 1.4 s.**

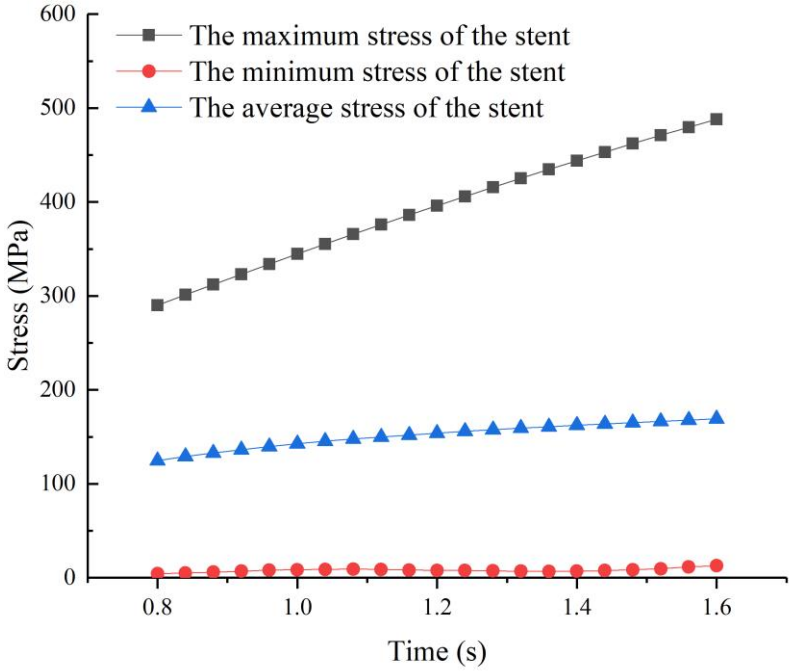

Figure 12 Maximum, minimum, and average stresses of the stent during 0.8~1.6 s.

3.4 Blood flow rate and endovascular wall pressure after maximum stent expansion

In this section, the blood flow velocity distribution in the XOZ plane at t = 4s has been analyzed (see Figure 13 (A), (B)). Compared with Figure 4 the blood flow rate increases exponentially since most of the flow channel at the stenosis is occupied by the balloon and stent system. The blood flow rate decreases and is close to zero in the non-stenotic region downstream of the implant, as well as at the regions close to the interface of the stent system and the vascular wall. However, the corresponding pressures on the endovascular wall (see Figure 13 (C)), show a sharp increase at the entrance, and a sharp drop downstream of the stenotic region.

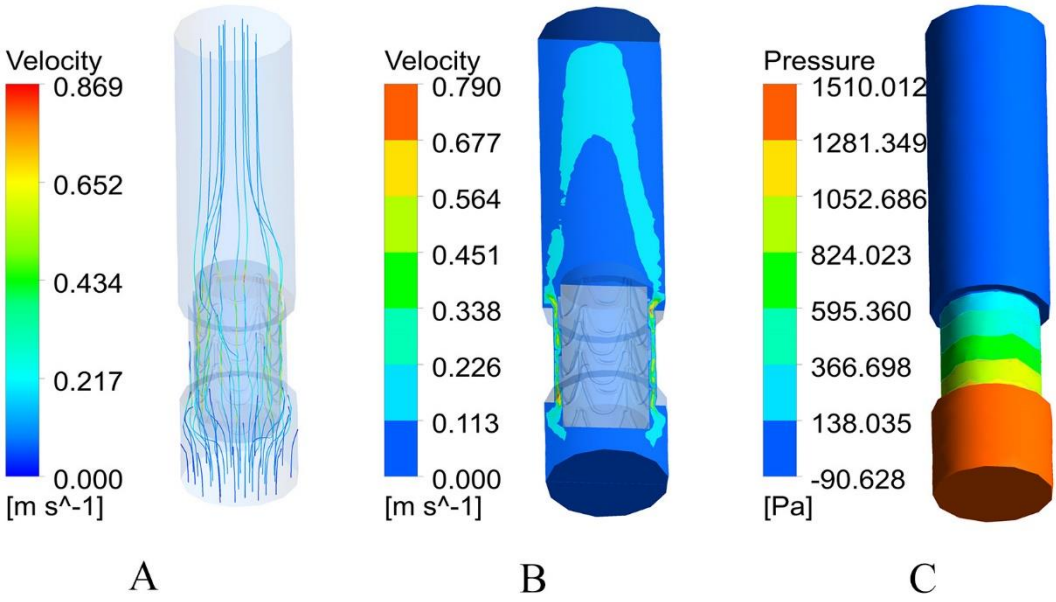

Figure 13 Blood flow velocity(A),(B) and vascular wall pressure(C) cloud diagrams at t = 4s.

4 Discussion and conclusion

This paper presents a simulation of the stent expansion process for a balloon-expandable coronary stent implanted for a vascular stenosis using finite element methods. The blood flow distribution and velocity in the vessel at t = 0.8 s, 1.0 s, and 1.4 s during the stent expansion process were analyzed. To obtain more accurate results, the blood flow distribution and velocity in a vessel without an implant was used as the control. The results show that at the same time point and the same inlet blood flow rate, the maximum blood flow rate at the stenosis increases significantly due to the effect of balloon and stent. Moreover, the blood flow in a small region downstream of the implant is disturbed and the blood flow returns to normal after passing through this region.

Due to the effect of the blood flow rate and its distribution, the pressure distribution on the endovascular wall varies accordingly. By analyzing the cloud diagrams of the pressure on the endovascular wall at t = 0.8 s, 1.0 s, and 1.4 s, the following conclusions were drawn: as blood flow rate increases, the maximum pressure of blood on the endovascular wall increases, while the pressure drops rapidly along the axis of the vascular wall; due to the presence of an implant, the pressure on the endovascular wall changes sharply at both the entrance and the stenotic region.

When the blood flow encounters the stent, pressure is generated on the surface of the stent. To analyze the mutual effects, cloud diagrams for the pressure on the stent system at t = 0.8 s, 1.0 s, and 1.4 s have been analyzed and compared with the internal stress of the stent. The results show that the blood load produces a maximum pressure of hundreds of Pascals on the surface of the stent, but this pressure is 10^6 times different from the equivalent stress of several hundred MPa, at the same time point. Therefore, the internal stress analysis of the stent should first consider its geometric bends, where the maximum stress usually occurs. In the limiting condition, the blood load can be ignored when analyzing the internal stress of the stent.

The expansion of the balloon-stent system can affect the blood flow distribution in a vessel, which in turn affects the pressure on the endovascular wall. By comparing the blood flow distribution and pressure on the vascular wall at t = 0.8 s and t = 4.0 s, the following results were obtained: the more space the implant occupies, the faster the blood flow rate at the stenosis, and the greater the pressure on the vascular wall; the pressure on the vascular wall changes drastically along the axis of the blood vessel. Therefore, in the process of clinical stent implantation, the duration of the surgery should be shortened as much as possible to reduce the effects of the implant on the blood vessel, and the harm to the human body from the resulting elevation in blood pressure. In particular, for patients with arteriosclerosis and greater than normal calcification of blood vessel walls, the higher blood pressure resulting from stent implantation increases the risk of rupturing the vascular wall.

Conflict of Interest

The authors declare that the research was conducted in the absence of any commercial or financial relationships that could be construed as a potential conflict of interest.

Author Contributions

SB, and HL presented the concept of the work. SB performed the FEA and CFD computations and drafted the manuscript. LL analyzed the data and drew the figures. HL provided suggestion and editing assistance.

Data availability statement

All datasets generated in the study are included in the article, further inquiries can be directed to the corresponding authors.

Ethics statements

No animal studies are presented in this manuscript.
No human studies are presented in this manuscript.
No potentially identifiable human images or data is presented in this study.

Reference

1 Koens, M.J., Krasznai, A.G., Hanssen, A.E., Hendriks, T., Praster, R., Daamen, W.F., et al. (2015). Vascular replacement using a layered elastin-collagen vascular graft in a porcine model: one-week patency versus one-month occlusion. Organogenesis. 11 (3), 105-121.doi:10.1080/15476278.2015.1038448

2 Lim, S.S., Gaziano, T.A., Gakidou, E., Reddy, K.S., Farzadfar, F., Lozano, R., et al. (2007). Prevention of cardiovascular disease in high-risk individuals in low-income and middle-income countries: health effects and costs. The Lancet. 370 (964), 2054-2062.doi:10.1016/S0140-6736(07)61699-7

3 Zhang, L.P., Liu, J.X. (2007). Progress on research of drug-coated stent. Journal of Biomedical Engineering. 24(1), 235-239.doi: 10.1097/01.crd.0000200844.16899.fc.

4 Wei, Z.Y., Liu, L., Qi, M. (2010). Progress in researches of biodegradable intravascular stents. Journal of Biomedical Engineering. 25(05), 1226-1230.doi: 10.1007/s10330-008-0032-0

5 Wu, T.Y., Ham, S.W., Katz, S.G. (2014). Predictors and consequences of hemodynamic instability following carotid artery stenting. Annals of Vascular Surgery. 60 (2), 543-543. doi:10.1016/j.jvs.2014.05.071

6 Wang, H.Q., Wang, S.B., Liu, K.D., Xing, Y.Q. (2017). Effects of local hemodynamics on carotid atherosclerotic plaque. Journal of Apoplexy and Nervous Diseases. 34 (07), 667-669. doi:10.1016/B978-0-7506-9603-6.50017-3

7 Bukač, M., Čanić, S., Muha, B. (2016). A nonlinear fluid-structure interaction problem in compliant arteries treated with vascular stents. Applied Mathematics & Optimization, 73(3), 433–473. doi:10.1007/s00245-016-9343-7

8 Qiao, A., Zeng, K. (2013). Numerical simulation of hemodynamics in intracranial saccular aneurysm treated with an ovel stent. Neurological Research, 35 (7), 701–708. doi:10.1179/1743132813Y.0000000186

9 Jang, S., Stevens, T., Chahal, P., Bhatt, A., Vargo, J. (2018). Comparative efficacy of lumen apposing metal stent versus fully covered self-expandable metallic stent in the management of pancreatic fluid collection. Gastrointestinal Endoscopy, 87 (6), 394–395.doi:10.1016/j.gie.2018.04.1858

10 He, Y.N., Lin, C.Y. (2015). Effects of wall shear stress on coronary stent restenosis. Chinese Journal of Biomedical Engineering. 34 (3), 354-359. doi:10.3969/j.issn.0258-8021.2015.03.013

11 Jiang, X.D., Teng, X.Y., Shi, D.Y., Zhang, Y.F. (2016). Numerical simulation research on mechanical behavior of intervention coupling systems for coronary stents. Engineering Mechanics. 33(8), 231-237.doi:10.6052/j.issn.1000-4750.2014.12.1050

12 Zhang, Y.P., Zhou, M., Tang, W.H. (2017). Numerical simulation of hemodynamics in a bioresorbable vascular scaffold. Chinese Journal of Tissue Engineering Research. 21(34), 5532-5537. doi:10.3969/j.issn.2095-4344.2017.34.020

13 Natarajan, S., Mokhtarzadeh-Dehghan, M.R. (2000). A numerical and experimental study of periodic flow in a model of a corrugated vessel with application to stented arteries. Medical Engineering & Physics. 22, 555–566.doi:10.1016/S1350-4533(00)00072-2

14 Ladisa, J.F., Guler, I., Olson, L.E., Hettrick, D.A., Kersten, J.R., Warltier, D.C., et al. (2003). Three-dimensional computational fluid dynamics modeling of alterations in coronary wall shear stress produced by stent implantation. Annals of Biomedical Engineering. 31(8), 972-980.doi:

15 Seo, T., Schachter, L.G., Barakat, A.I. (2005). Computational study of fluid mechanical disturbance induced by endovascular stents. Annals of Biomedical Engineering. 33(4), 444-456.doi:10.1007/s10439-005-2499-y

16 Martina, Bukač., Sunčica, Čanić., Muha B. (2016). A nonlinear fluid-structure interaction problem in compliant arteries treated with vascular stents. Applied Mathematics and Optimization. 73(3), 433-473.doi:10.1007/s00245-016-9343-7

17 Bukac, M., Čanić, S. (2019). Fluid–structure interaction between pulsatile blood flow and a curved stented coronary artery on a beating heart: A four stent computational study. Computer methods in applied mechanics and engineering. 350, 679-700.doi:10.1016/j.cma.2019.03.034

18 Jayendirana, R., Nourb, B., Ruimia, A. (2019). Computational analysis of Nitinol stent-graft for endovascular aortic repair (EVAR) of abdominal aortic aneurysm (AAA): Crimping, sealing and fluid-structure interaction (FSI). International Journal of Cardiology. 304, 167-171.doi:10.1016/j.ijcard.2019.11.091

19 Jayendirana, R., Nourb, B., Ruimia, A. (2018). Fluid-structure interaction (FSI) analysis of stent-graft for aortic endovascular aneurysm repair (EVAR): Material and structural considerations. Journal of the Mechanical Behavior of Biomedical Materials. 87, 95-110.doi:10.1016/j.jmbbm.2018.07.020

20 Leea, W., Chob, S.W., Usaid, K. (2020). Allahwalac and Ravinay Bhindic. Numerical study to identify the effect of fluid presence on the mechanical behavior of the stents during coronary stent expansion. Computer Methods in Biomechanics and Biomedical Engineering.doi: 10.1080/10255842.2020.1763967

21 Shi, G.Q., Song, X.B. (2015). Finite element analysis of intravascular stent based on ANSYS software. Journal of Biomedical Engineering. 32(05), 1004-1008.doi:10.7507/1001-5515.20150178

22 Timmins, L.H., Moreno, M.R., Meyer, C.A., Criscione, J.C., Rachev, A., Moore, J.E. (2007). Stented artery biomechanics and device design optimization. Medical & biological engineering & computing. 45(5), 505-513.doi:10.1007/s11517-007-0180-3

23 Zheng, Y.F., Yang, H.T. (2017). Research progress in biodegradable metals for stent application. Acta Metallurgica Sinica. 53, 1227-1237.doi:10.11900/0412.1961.2017.00270

24 Li, J., Peng, K., Cui, X.Y., Fu, W.Y., Qiao,A. (2018). Numerical simulation of the effect of virtual stent release pose on the expansion results. Journal of Biomedical Engineering. 35(2), 214-218.doi:10.7507/1001-5515.201703013

25 Li, H.X., Zhang, Y.H., Wang, X.C. (2012). Analysis of stent expansion, blood flow and fatigue life based on finite element method. Journal of Medical Biomechanics. 27(2), 178.doi：10.3871/j.1004-7220.2012.02.185.

26 Cebral, J., Mut, F., Sforza, D., Putman, C. (2011). Clinical application of image-based CFD for cerebral aneurysms. International Journal for Numerical Methods in Biomedical Engineering. 27(7), 977-992.doi:10.1002/cnm.1373

Figures

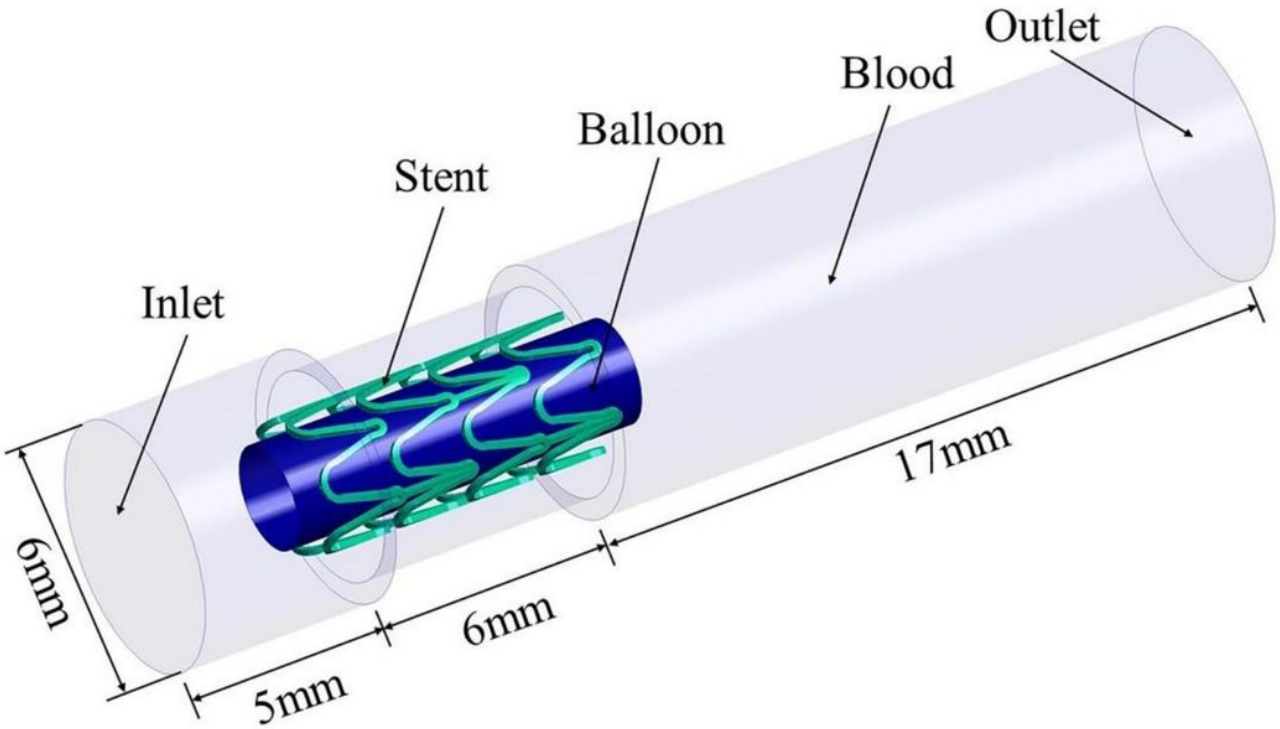

Figure 1

A combined model of the balloon, stent, and blood vessel.

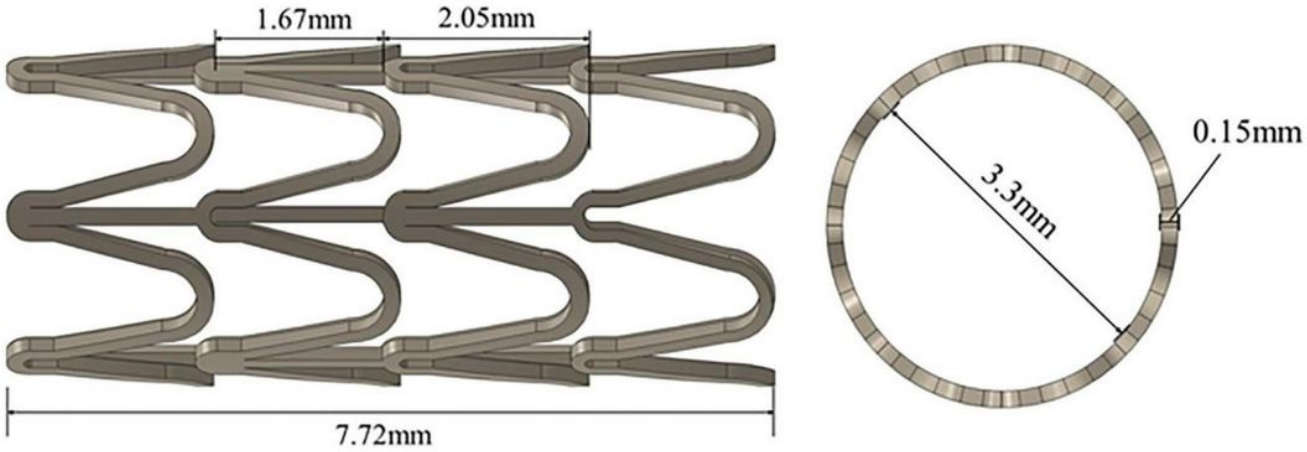

Figure 2

Model of the stent.

Figure 3

Meshes for the balloon-expandable stent (A) and blood (B).

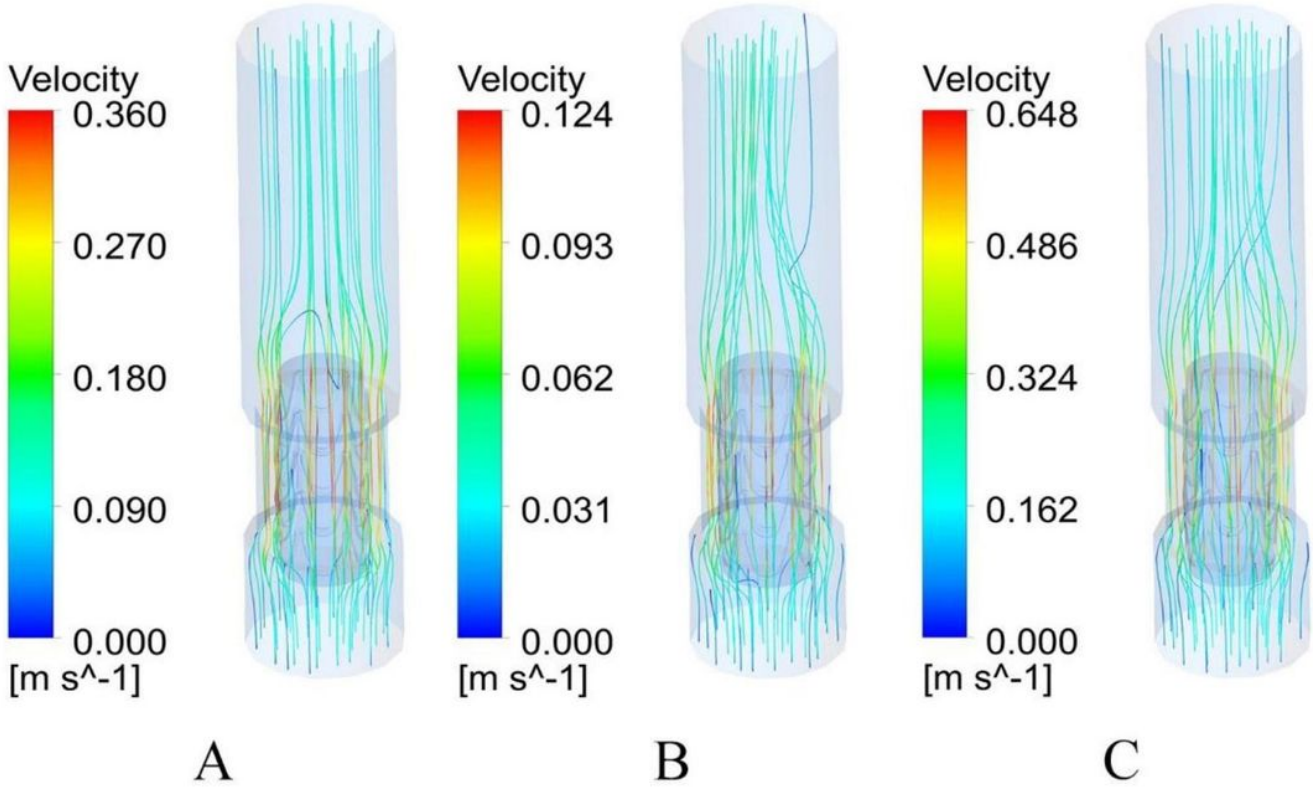

Figure 4

Blood flow velocity streamline diagram during stent expansion at t = 0.8 s(A), 1.0 s(B), and 1.4 s(C).

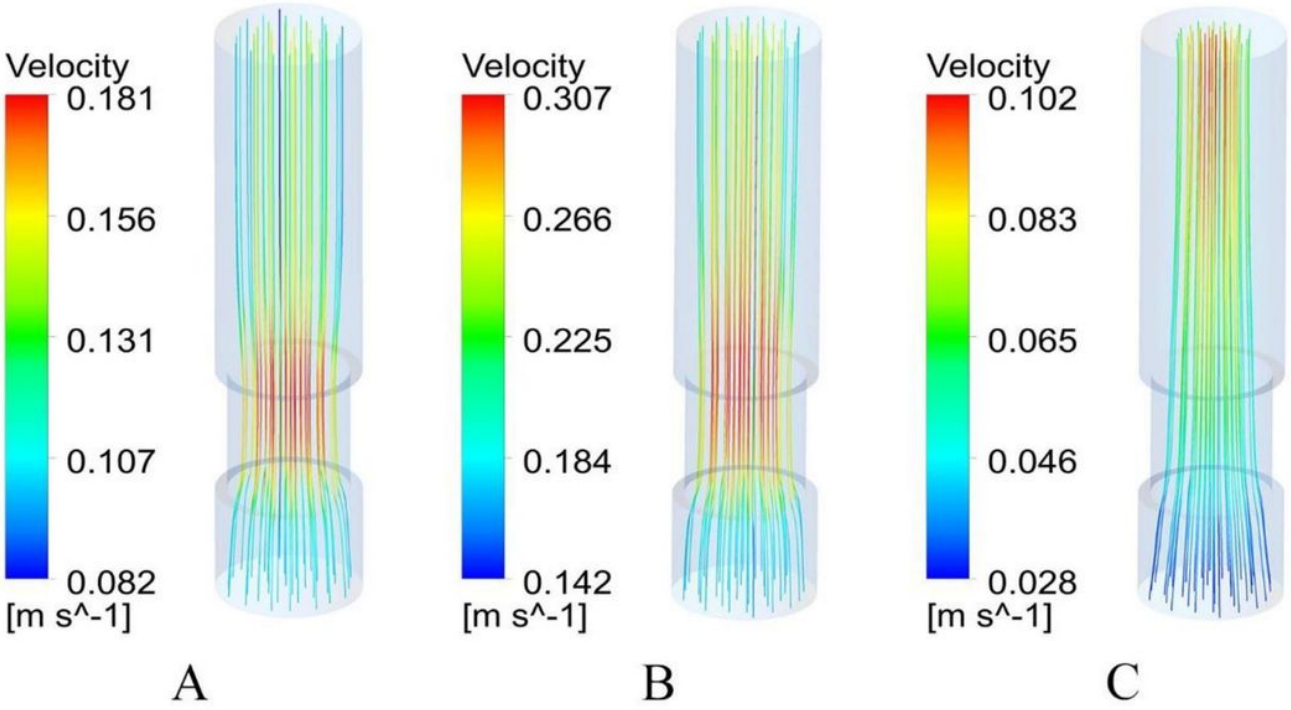

Figure 5

Blood flow velocity streamline diagram without stent at t = 0.8 s(A), 1.0 s(B), and 1.4 s(C).

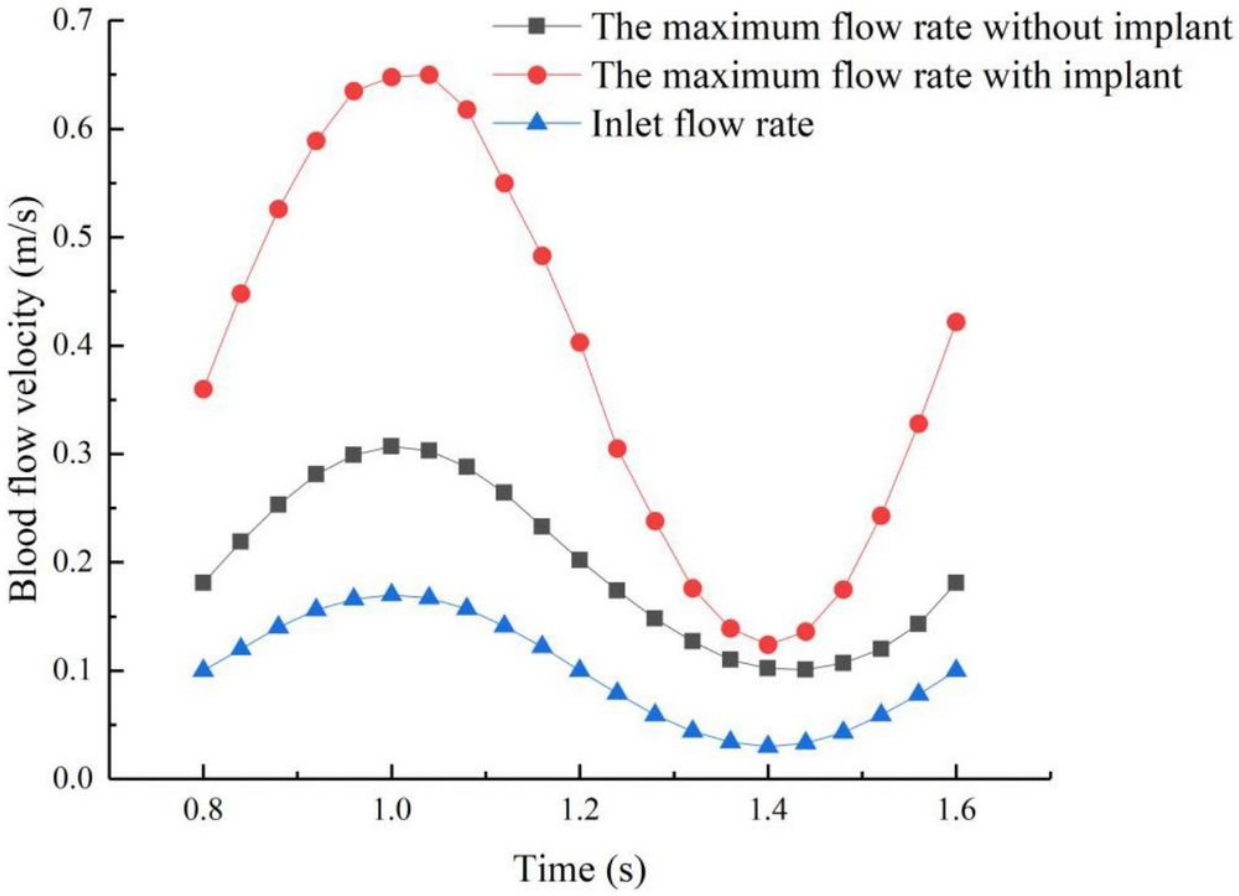

Figure 6

Inlet blood flow rate, and maximum blood flow rate with and without implant at 0.8~1.6s.

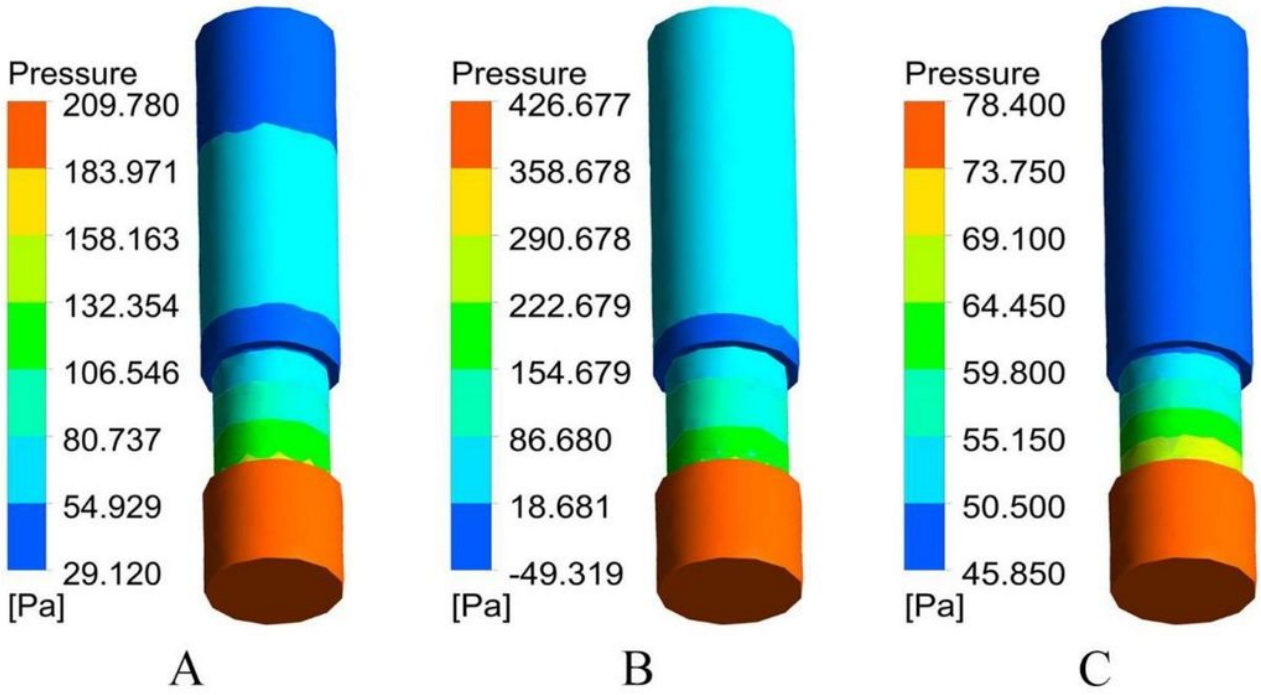

Figure 7

Pressure distributions at the endovascular wall during stent expansion at t = 0.8 s(A), 1.0 s(B), and 1.4 s(C).

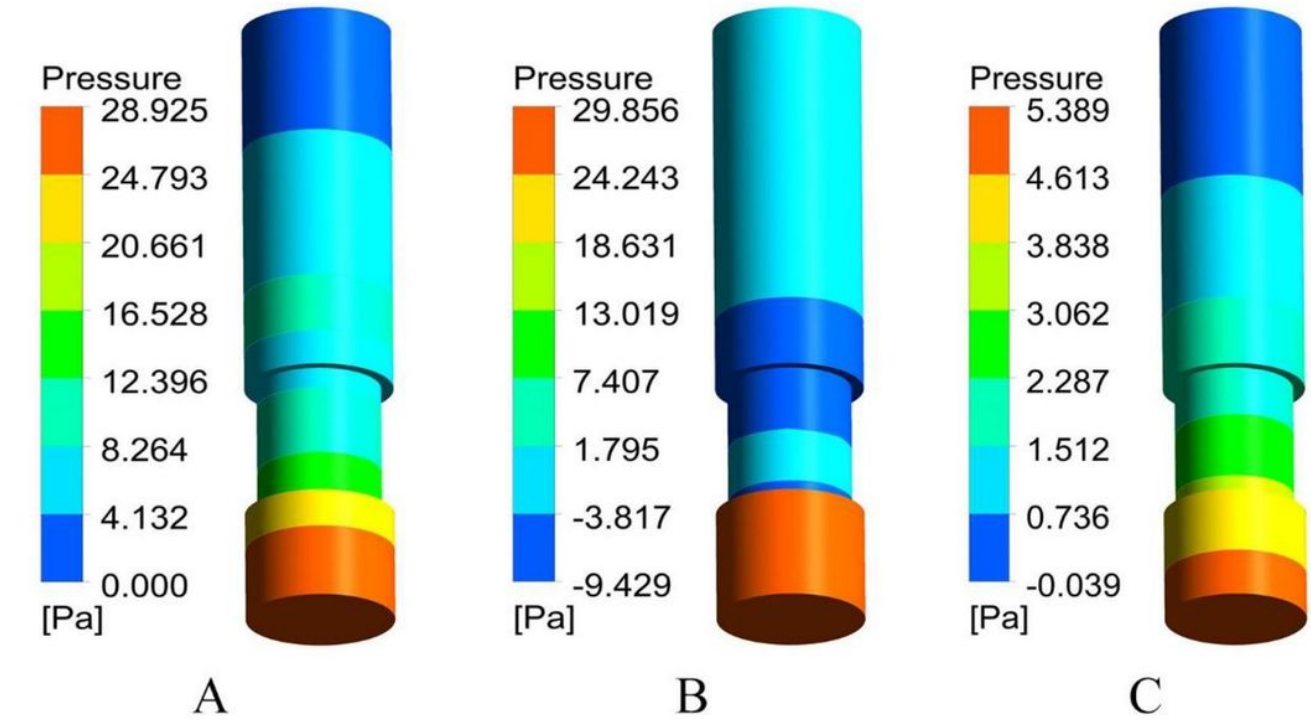

Figure 8

Pressure distributions at the endovascular wall at t = 0.8 s(A), 1.0 s(B), and 1.4 s(C) without stent.

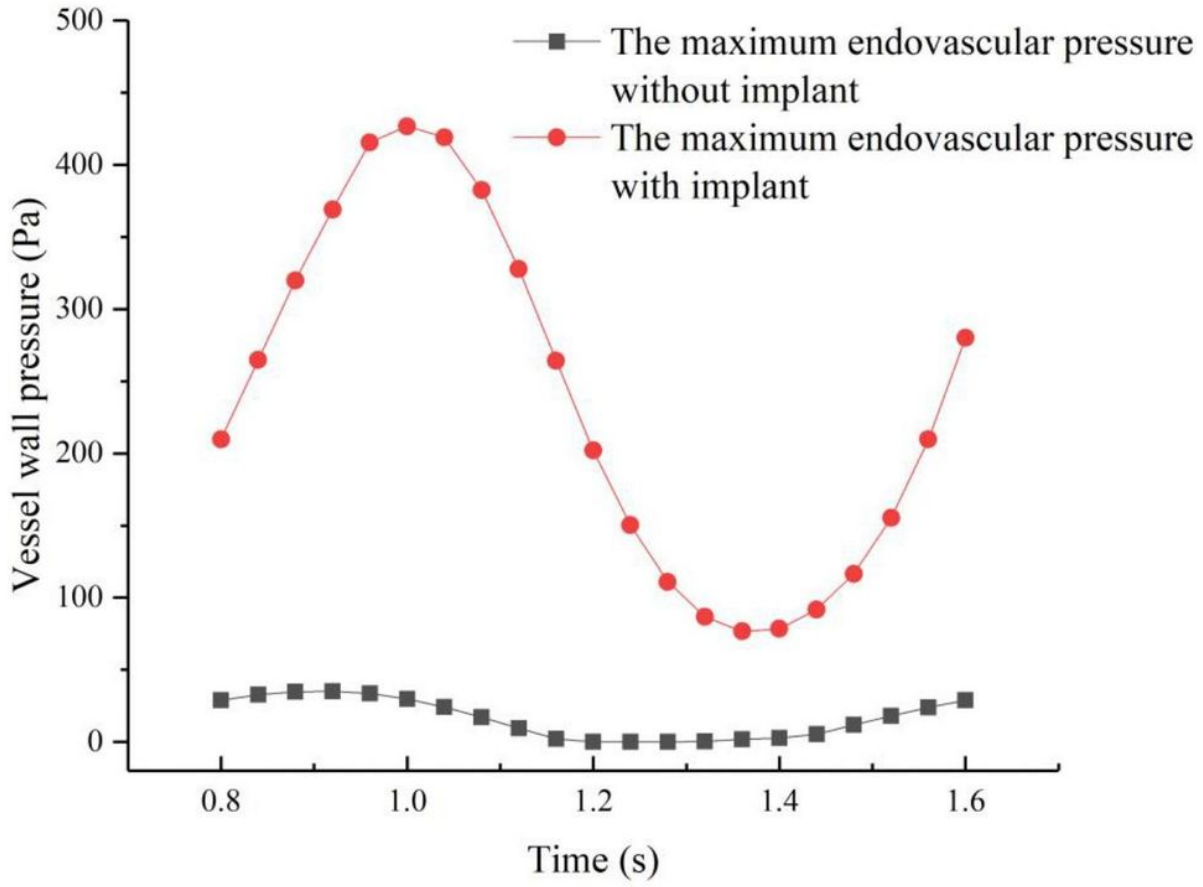

Figure 9

Maximum pressure on the endovascular wall during 0.8~1.6 s with and without implant

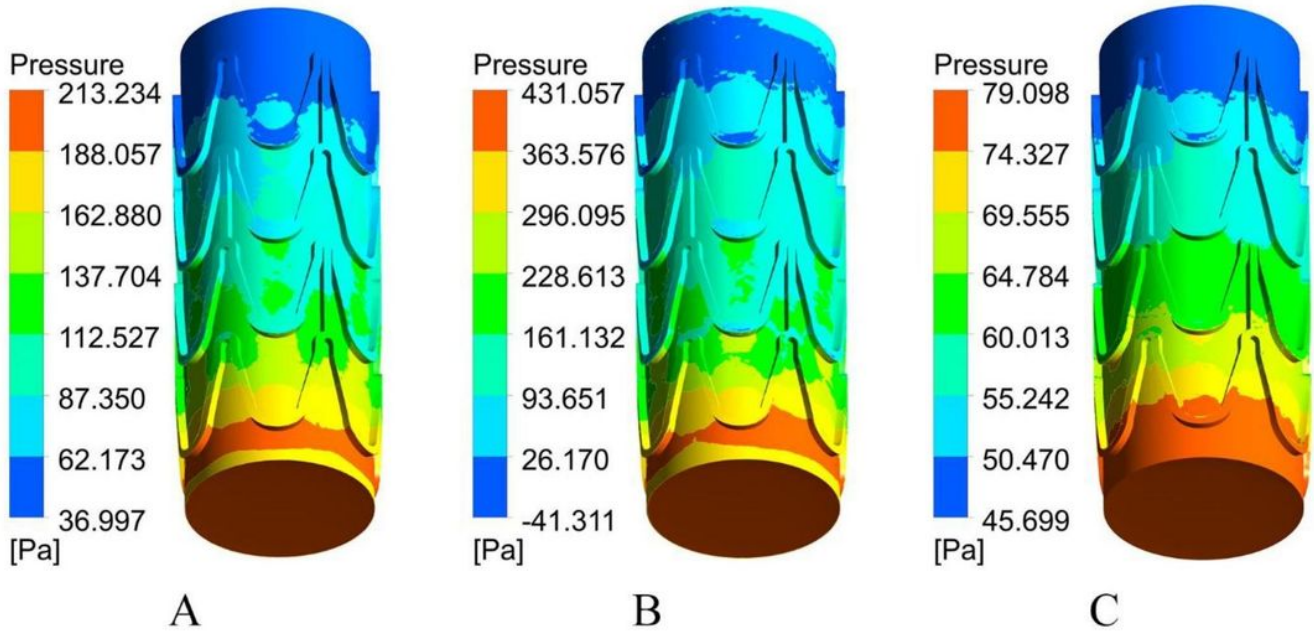

Figure 10

Pressure distribution of the stent system at t = 0.8 s(A), 1.0 s(B), and 1.4 s(C).

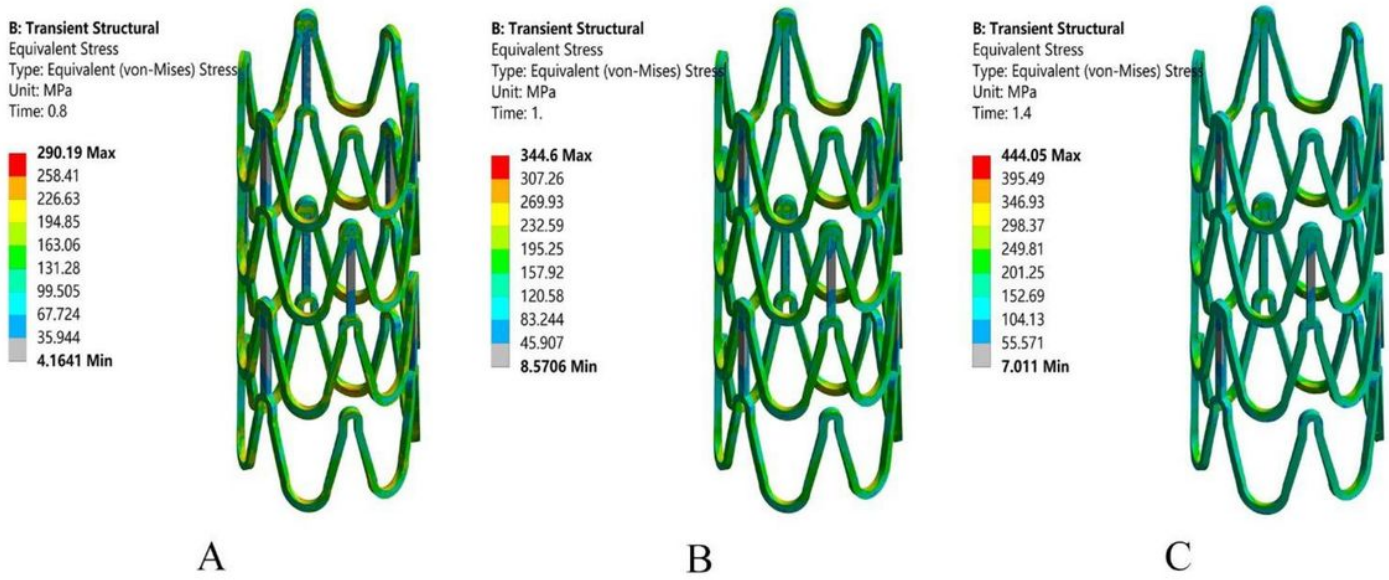

Figure 11

Equivalent stresses of the stent at t = 0.8 s, 1.0 s, and 1.4 s.

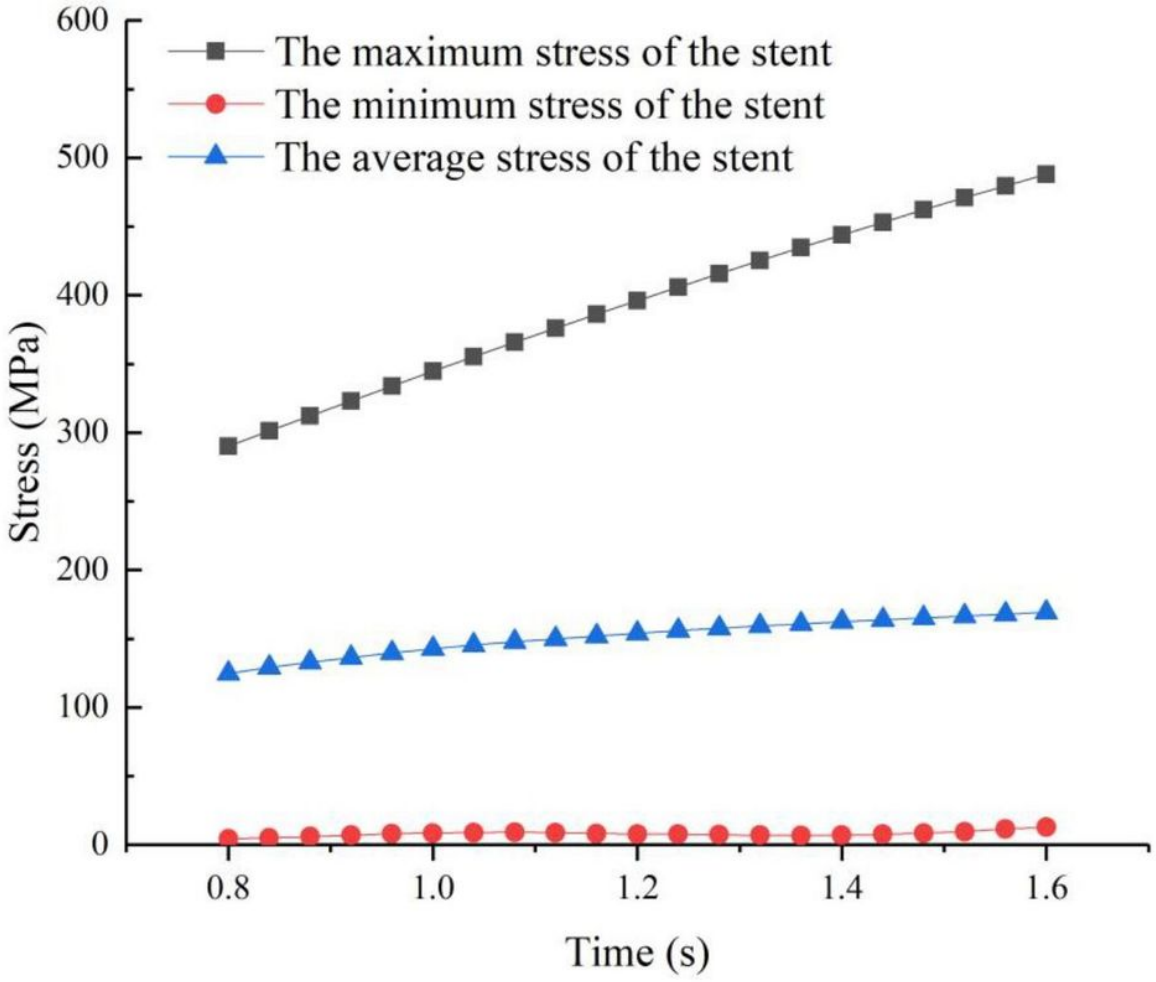

Figure 12

Maximum, minimum, and average stresses of the stent during 0.8~1.6 s.

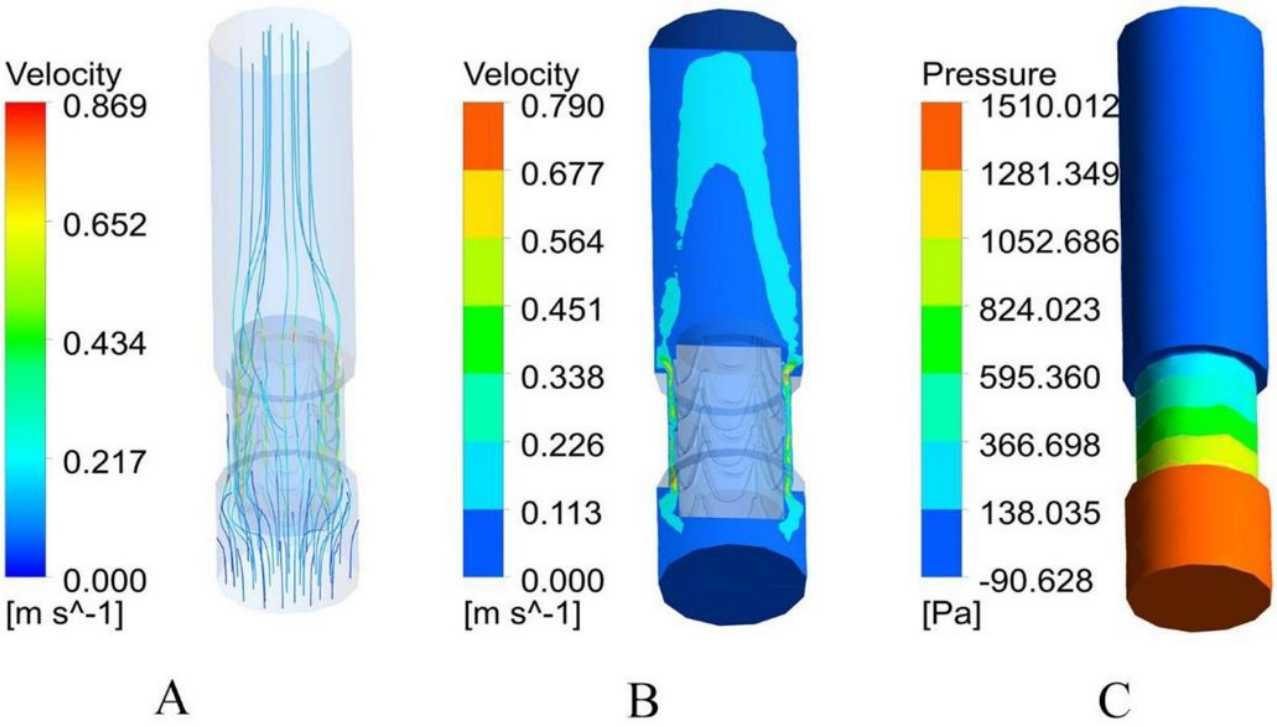

Figure 13

Blood flow velocity(A),(B) and vascular wall pressure(C) cloud diagrams at t = 4s.